Modeling of annual oscillations and 1/*f*-noise of daily river discharges

B. M. Dolgonosov, K. A. Korchagin, N. V. Kirpichnikova

Water Problems Institute, Russian Academy of Sciences,

3 Gubkina, Moscow 119333, Russia

Abstract. A frequency dependence of river runoff power spectrum is deduced from the integrated runoff and storage dynamics, derived from the mass and momentum balance equations for the water on a river catchment. The power spectrum consists of three multipliers: a $1/f^{\beta}$ noise factor with $\beta \sim 1$ reflecting a stochastic behavior of precipitation; a Lorentzian factor $1/(f_c^2 + f^2)$ damping high-frequency runoff oscillations; and the sum of spectral modes of annual and intra-annual periodicity. This spectrum has two different power-law trends, separated by the crossover frequency f_c, with the exponents β and $\beta + 2$ at low and high frequencies respectively. The theoretical results are tested on four discharge time series (3580 to 6575 daily records) of the river Volga at Staritsa and three rivers of the Volga basin, catchment areas varied from 1850 to 21100 km^2. The time series are used to calculate empirical power spectra of river discharges and to construct the theoretical power spectra by fitting model parameters to the data. The calculations indicate that the spectral exponent β is approximately equal to 1 for three rivers and to 0.67 for one river. The crossover frequency f_c corresponds to a period of 12 days for large catchment areas and ~3 days for small one. The comparison shows that the model and empirical spectra by their spectral trends at low and high frequencies, crossover frequency, and positions of first several spectral modes are in satisfactory agreement. To isolate an effect of fluctuations, we consider a transformed runoff time series for one of the rivers, obtained by subtraction of the multiyear average daily hydrograph from the raw time series. The transformed time series interpreted as discharge fluctuations is used to calculate the fluctuation power spectrum. This spectrum has two different power-law trends with a spectral exponent of 0.6 at low frequencies and 2.7 at high frequencies. The difference is about 2 like for the power spectrum of raw time series, but the crossover frequency slightly moves to a value corresponding to a period of 15 days.

Keywords: Runoff dynamics; Fourier transform; Power spectra; Scaling; Power-law trends; Crossover frequency

1. Introduction

Spectral analysis is a convenient instrument for drawing important information from river runoff time series concerning runoff oscillations and some generalized characteristics of river catchment and precipitation. In particular, spectral analysis yields the least biased results and the lowest variance in its estimates of the fractal dimension (Schepers et al., 1992).

It has been revealed in a series of works (Tessier et al., 1996; Pelletier and Turcotte, 1997; Pandey et al., 1998; Neal and Kirchner, 2000; Dahlstedt and Jensen, 2003; Feng et al., 2004; Koscielny-Bunde et al., 2006) that runoff power spectra include discrete components on the background of fluctuations in the form of 1/*f*-noise. Correlation functions of these fluctuations have a power-law dependence on time lag (Beran, 1994) that is typical for fractional Gaussian noises introduced by Mandelbrot and Wallis (1968). The power-law dependence suggests long-range persistence of correlations. This contrasts with autoregressive models which have correlation functions exponentially decaying with time lag. A little earlier Hurst et al. (1965) have found that a variety of climatological and hydrological time series produce a power-law rescaled-range plot with an average exponent of $H = 0.73$. Bras and Rodriguez-Iturbe (1985) have shown that a fractional Gaussian noise with a power-law exponent of –1/2 yields a power-law rescaled-range plot with exponent $H = 0.75$, close to the value observed by Hurst et al. (1965).

Pelletier and Turcotte (1997) calculated power spectra of time-series data for river discharges (636 monthly records) and precipitation (49 annual records) averaged over hundreds of stations worldwide. The average power spectrum *S* of river discharges has a power-law dependence on frequency $S(f) \sim f^{-1/2}$ for time scales from 1 month to 10 years. However, for the precipitation power spectrum there is no identifiable persistence at time scales less than 10 years. The presence of long memory for river discharges as implied by the power-law trend of the spectrum has a significant effect on the occurrence of extreme events compared to standard autoregressive models with short memory.

It is known (Whittle, 1962) that some stochastic partial differential equations yield solutions with long-range persistence in space and time. Random processes with long-range correlations and 1/*f*-noises in power spectra have probability distributions with heavy tails (Vladimirov et al., 2000). As shown by Naidenov (2004), Dolgonosov and Korchagin (2005, 2007), and Dolgonosov et al. (2006), this sort of probability distributions for river discharges and water quality indices can be deduced from some stochastic ordinary differential equations. Long-term persistence was directly observed in the decay of organic matter in water (Dolgonosov and Gubernatorova, 2005, 2007).

Feng et al. (2004) considered 17-year weekly data series of the river Hafren at Plynlimon, Wales, and showed how spectral analysis of long-term hydrological and hydrochemical data can be

used to infer the travel-time distribution of water through catchments, and to measure the chemical retardation of reactive solutes at the catchment scale. They demonstrated that high-frequency sampling (e.g., daily or more frequent) is particularly useful for revealing the short-term chemical dynamics that most clearly reflect the interplay of subsurface chemical and hydrological processes. The authors revealed that fluctuations of travel times are more strongly damped in the stream compared to precipitation. This was also noted by Neal and Kirchner (2000). The chemical power spectrum scales as a white noise in rainfall and as a 1/*f*-noise in streamwater.

Baldwin and Lall (1999) investigated the seasonality in streamflows. They studied a 123-year record of daily flows and presented evidence for changes in the timing and amplitude of seasons.

Based on the spectral analysis of annual river flow, rainfall, temperature, and tree-ring data in the midwestern United States (sample sizes: river flow, 62 to 119 annual records for each of 26 stations; rainfall and temperature, 72 to 114 records, 36 stations; tree-ring, 211 to 513 records, 22 locations) and using the multi-taper method of spectral analysis, Rao and Hamed (2003) observed perennial oscillations in all the data having the common periodicities of 2.5–2.6, 3–3.5, 5–6, and 10.7–11.1 years. It was also found that there are periodicities of 17.9–19.6 and 60–69 years in temperature data, 21–26 years in river flow data, and 32–34 years in rainfall data. The authors noted that there is considerable evidence for drifts in these periodic components.

Pekarova et al. (2003) used the interannual spectral analysis to test selected large rivers in the world for wet and dry periods. They used annual discharge series with time scales from several decades to nearly two hundred years and demonstrated the existence of long-term discharge fluctuations (20–30 years) and a shift in the occurrence of long-term runoff extremes over the earth.

Koscielny-Bunde et al. (2006) studied temporal correlations and multifractal properties of river discharge records from 41 hydrological stations around the globe. They considered daily records of 51 to 171 years duration. To detect long-term correlations and multifractal behavior in the presence of trends, the authors applied the detrended fluctuation analysis as well as its multifractal realization and wavelet analysis. They found that above a crossover time of several weeks, daily runoffs are long-term correlated with the correlation function decaying as $C(\tau) \sim \tau^{-\gamma}$ with time lag τ. The exponent γ varies from river to river in a range of 0.1 to 0.9. The power-law decay of $C(\tau)$ corresponds to a power-law increase of the related fluctuation function $F_2(\tau) \sim \tau^{H}$ with the Hurst exponent $H = 1 - \gamma/2 = (1+\beta)/2$, where β is the exponent in the scaling of the runoff power spectrum with frequency $S(f) \sim f^{-\beta}$.

Tessier et al. (1996) studied power spectra of thirty French rivers having areas between 40 and 200 km^2, based on daily river runoff time series from 1 day to 30 years. They showed

multifractal nature of river runoffs with two frequency regions having a crossover at a period of about two weeks interpreted as the synoptic maximum (Koloshnikova and Monin, 1965). The ensemble averaged spectral exponent was estimated as $\beta = 1.3$ for the 1 to 16 days regime and $\beta = 0.52$ for the 1 month to 30 years regime of river runoff.

Pandey et al. (1998) analyzed daily streamflow data from 19 gauging stations from the continental USA. The length of the data series varies from 3422 to 26663 days. The river flow series demonstrated a multifractal behavior over a range of scales spanning 2^3 to 2^{16} days. For most of the rivers, there is a break in the scaling regime at a period of about one week which is half the atmospheric synoptic maximum. For the scales longer than 8 days, the universal multifractal parameters characterizing the infinite hierarchy of scaling exponents were estimated. The spectral exponent for the low frequency region varied from $\beta = 0.73$ to 1.88 with an average value of 0.72 for the normalized ensemble. Although the basin areas varied over nearly six orders of magnitude, the scaling results were independent of the basin size and geology. Meanwhile, the influence of annual cycle was disregarded in (Tessier et al., 1996) and (Pandey et al., 1998).

Dahlstedt and Jensen (2003) described power spectra of daily river flow time series from 1 day to 3 years for two large river systems: the Danube and the Mississippi. The power spectra have two different frequency regimes of power-law-like nature separated by a crossover frequency f_c with the spectral exponent values of $\beta = 1$ and 3 at low and high frequencies respectively. For the Mississippi sites all the power spectra are similar and exhibit $1/f$ behavior down to the lowest recorded frequencies. For the Danube sites f_c changes with basin area. At low frequencies the spectra behave like $1/f$. With increasing basin area, f_c decreases and the spectrum moves towards a Lorentzian-like form $(f_c^2 + f^2)^{-1}$. This implies exponentially decaying time correlations with a characteristic decay time $\tau_c = 1/f_c$.

Hubert et al. (2002) analyzed daily flow time series of the Blavet river at Guerledan for the period from 1939 to 1999. This Celtic river exhibits much stronger intermittent spikes than other rivers. The spectral exponent was estimated as $\beta = 1.3$ for time-scales shorter than a year. In contrast to the observations of Tessier et al. (1996), Pandey et al. (1998) and Labat et al. (2002), the authors did not observe any peculiarities of the spectrum behavior on time-scales of the order of two weeks.

In the above-mentioned works, the $1/f$-noise was found empirically, from runoff series data, the presence of Lorentzian was guessed by the effect of changing the trend exponent by about two units at the crossover between different frequency regimes, but spectral components at the annual frequency and multiple frequencies remained out of the scope at all. By this cause, the objective of our work is to derive an analytical expression for runoff power spectrum based on runoff dynamics

at the catchment scale. To succeed in doing that, we will hold to the following programme: (i) to formulate dynamic equations for water storage and runoff; (ii) to linearize the equations in the neighborhood of a steady state; (iii) to apply the Fourier transform to the linearized equations for finding relationships for spectral densities; (iv) to determine the runoff power spectrum. The derived theoretical relationships are then applied to the description of spectra calculated from the water discharge time series for the river Volga at Staritsa and three more rivers of the Volga basin. Further, the model parameters are found and their possible links with catchment and precipitation characteristics are discussed.

2. Model

2.1. Integrated runoff dynamics

A river catchment can be represented schematically as a dense network with permanent and temporal streams of different orders, maybe including some lakes and reservoirs. An effective water storage of catchment can be defined as the water volume V taking part in runoff formation. It includes water volume within the river network, working volumes of reservoirs and lakes as well as volumes of mobile subsurface waters. Introduce a specific water storage and runoff as $h = V / A$ and $q = Q / A$ respectively, where A is the catchment area, Q is the water discharge through the catchment's closing site. The variables h and q will be called also 'water layer' and 'runoff layer' respectively. Now we consider integrated runoff dynamics in terms of the specific variables.

The atmospheric water precipitating onto the surface of landscapes is transferred by overland flow into the branching river network, where it is transported by channel flows.
It was found that in river basins formed on sedimentary rocks, the flow velocity tends to be constant throughout the river network (Rinaldo et al., 1993, 2006). This is due to the fact that the entire preceding erosion process of network formation proceeded in the direction of the minimum of energy dissipation. This fact is of exceptional importance for the description of runoff dynamics, because it allows a certain characteristic flow velocity u to be assigned to the river network, and local deviations from this value to be considered small fluctuations. Analogously, the relief slopes and friction forces can be characterized by their total mean values I and F on the background of fluctuations. The momentum balance equation in the line of the resulting water momentum of the catchment can be written in terms of the mean values as (Dolgonosov and Korchagin, 2007)

$$\frac{dmu}{dt} = mgI - F - J\,, \qquad (1)$$

where $m = \rho V = \rho h A$ is the effective (runoff-forming) mass of water on the catchment, ρ is the water density, g is the acceleration of gravity, $J = u\rho Q$ is the momentum flux through the closing site.

The friction force F depends on the flow velocity u and on resistances distributed by catchment area A. This dependence is commonly represented in the form (Landau and Lifshitz, 1986)

$$F = \lambda \rho u^2 A, \qquad (2)$$

where λ is a friction coefficient. The total friction force comprises different resistances for overland and channel flows, for example, such as the resistances in flows over a rough soil surface and in flows about obstacles in the vegetation cover (grass, brush, tree trunks, etc.). Since the integrated catchment runoff is considered, the details of individual processes are averaged and only generalized characteristics as the water layer h and the flow velocity u remain actual. They can be combined in a generalized Reynolds number

$$\mathrm{Re} = \frac{uh}{\nu},$$

where ν is the kinematic viscosity of water. The dependence of the friction coefficient λ on Re can be written in the form common for different types of flows (Batchelor, 1970; Spitsyn and Sokolova, 1990):

$$\lambda = \lambda_0 \, \mathrm{Re}^{-\beta}. \qquad (3)$$

If the overland flows give a prevailing contribution to the total catchment resistance, then $\beta = 1$ and the friction force linearly depends on flow velocity

$$F = \lambda_0 \rho \nu u A / h.$$

If the channel flows give a noticeable or crucial contribution to the total resistance, then $\beta < 1$ and β can take values down to zero.

Examples of dependence (3) for some model cases are represented in Table 1 (in each case the Reynolds number has its own specific features). In the case of a channel flow, we took into account, first, the relationship $\lambda \sim C^{-2}$ with the Chezy coefficient C; second, the dependence of Chezy coefficient on hydraulic radius (which in this case is equal to h): $C \sim h^{1/6}$ according to Manning and $C \sim h^{1/5}$ according to Forchheimer (Spitsyn and Sokolova, 1990); and, third, the proportionality $h \sim \mathrm{Re}$. All this results in the dependencies presented in the last two rows of Table 1.

The examples considered above are a heuristic evidence in favor of dependence (3). They show that different values of β from the range $\beta \in [0, 1]$ are possible. At arbitrary β from this range, relationships (2) and (3) yield

$F = \lambda_0 \rho \nu^2 A \mathrm{Re}^{2-\beta} h^{-2}$.

Table 1. Friction coefficient as a function of Reynolds number at different types of flows

Flow type	Friction coefficient	References
Laminar flow	$\lambda \sim \mathrm{Re}^{-1}$	Batchelor, 1970
Turbulent flow about bodies	$\lambda \sim \mathrm{Re}^{-1/2}$	Batchelor, 1970
Turbulent flow in smooth pipes	$\lambda \sim \mathrm{Re}^{-1/4}$	Shih-I Pai, 1959
Flow about plate	$\lambda \sim \mathrm{Re}^{-1/5}$	Shih-I Pai, 1959
Channel flow by Manning	$\lambda \sim \mathrm{Re}^{-1/3}$	Spitsyn and Sokolova, 1990
Channel flow by Forchheimer	$\lambda \sim \mathrm{Re}^{-2/5}$	Spitsyn and Sokolova, 1990

The water discharge Q through the closing site is equal to the total runoff from the catchment. It can be determined by two ways: via the mean flow velocity u in the river network and via the runoff layer q:

$Q = uhB = qLB$,

where L and B are the catchment's length and width. From this it follows that

$uh = qL$.

Using the obtained expressions for F and J, replacing u into q in them, and inserting the result in (1), we get the runoff dynamic equation

$$\frac{dq}{dt} = ah - b\frac{q^{\mu}}{h^2} - \frac{q^2}{h}, \qquad (4)$$

where

$$a = \frac{gI}{L}, \quad b = \frac{\lambda_0 \nu^2}{L}\left(\frac{L}{\nu}\right)^{\mu}, \quad \mu = 2 - \beta.$$

Because $\beta \in [0, 1]$, then $\mu \in [1, 2]$.

Let us estimate individual terms in equation (4) at the values of parameters typical for a moderate-sized lowland river like the river Moskva in the period of spring tide with maximum discharge:

$Q \sim 10^3$ m^3/s, $V \sim 10^8$ m^3, $A \sim 10^{10}$ m^2, $I \sim 10^{-3}$, $\beta = 1$, $\lambda_0 \sim 1$.

This yields

$h = V/A \sim 10^{-2}$ m, $q = Q/A \sim 10^{-7}$ m/s, $L \sim B \sim \sqrt{A} \sim 10^5$ m, $u = Q/(hB) \sim 1$ m/s,

$ah \sim 10^{-9}$ m/s^2, $bq^{\mu}/h^2 \sim 10^{-9}$ m/s^2, $q^2/h \sim 10^{-10}$ m/s^2.

Thus, even in the period of spring tide the inertial term q^2/h has an order of magnitude less than the two other terms in the right-hand side of equation (4). At usual, not too high discharges the inertial term is still less significant, therefore it can be neglected and the runoff equation can be written in the simpler form

$$\frac{dq}{dt} = ah - b\frac{q^{\mu}}{h^2}. \qquad (5)$$

2.2. Local equilibrium: scaling between runoff and storage

The runoff from a catchment usually proceeds in local equilibrium conditions, when the action of gravity counterbalances with the friction force (Mantilla et al., 2006). The local equilibrium establishes due to the viscous dissipation of flow energy taking a relaxation time Δt that can be found, according to (5), from the relationship

$$\frac{\Delta q}{\Delta t} \sim b\frac{q^{\mu}}{h^2}.$$

Supposing $\Delta q \sim q$ and employing the above estimates, we get

$$\Delta t \sim \frac{h^2}{bq^{\mu-1}} \sim 10^2 \text{ s}.$$

Thus, the relaxation to local equilibrium water discharge lasts several minutes, whereas water storage changes over a longer period of time (measured at least by days) needed for draining the water from catchment. This means that q is a fast variable, which follows a slow change of the layer h.

The condition of local equilibrium implies that the derivative dq/dt is negligibly small. Putting in (5) $dq/dt = 0$, we obtain

$$ah - bq^{\mu}h^{-2} = 0.$$

This leads to a fundamental relationship between runoff and storage

$$q = kh^d, \qquad (6)$$

where

$$d = \frac{3}{\mu}, \quad k = \left(\frac{a}{b}\right)^{1/\mu} = \frac{\nu}{L}\left(\frac{gI}{\lambda_0 \nu^2}\right)^{1/\mu}. \qquad (7)$$

The exponent d can be eventually expressed through the exponent β in the friction law (3), which reflects the integrated runoff regime – laminar, turbulent, or intermediate, depending on contributions of the overland and channel flows to the total catchment resistance. The range of d

values can be easily found: $d \in [\frac{3}{2}, 3]$. The proportionality coefficient k, as follows from (7), is inversely proportional to the catchment length L and depends on the mean slope by a power law: $k \sim I^{1/\mu} L^{-1}$. It shows that the specific runoff increases with slope but decreases with catchment length because of the lag effect. The coefficient k determines runoff per unit storage. The reciprocal quantity $R \equiv k^{-1}$ can be called the 'catchment resistance'. There is an obvious analogy with electric current: the runoff q corresponds to the current I, and the involuted water storage h^d to the potential U, so that equation (6) is equivalent to the Ohm law $I = U / R$.

A power relationship like (6) was used in (Klemeš, 1973, 1974; Frolov, 1985; Naidenov, 2004). It was obtained in (Kuchment, 1980) by simplifying the Saint-Venant equations. Two extreme values of d were given there: $d = 3/2$ for a turbulent flow and $d = 3$ for a laminar one. The expressions for parameter k somewhat differ from (7). Relationship (6) with $d = 3/2$ for channel flows was also derived in (Mantilla et al., 2006) based on the Chezy equation.

Along with the above dynamic deduction, one can use simple geometric arguments also bringing to scaling (6). It is known that a river network represents a fractal object (Maritan et al., 1996; Banavar et al., 1997, 1999; Cudennec et al., 2003; Rinaldo et al., 2006). The feature of fractals is that their integral characteristics depend on object size by a power law. In application to such characteristics of river network as water storage and runoff, this means that $V \sim L^{\phi}$ and $Q \sim L^{\psi}$. Excluding L from these dependencies, we find a scaling of $Q \sim V^d$, where $d = \psi / \phi$. Turning from the integral quantities V and Q to the specific one h and q, we again come to relationship (6).

2.3. Integrated storage dynamics and linear approximation

Let us now consider water storage dynamics for the whole catchment. From the water balance on the catchment, we can easily obtain an integrated storage dynamic equation

$$\frac{dh}{dt} = p(t) - q, \qquad (8)$$

where $p(t) = [1 - \varphi(t)]w(t)$ is an effective precipitation rate, $w(t)$ is the precipitation rate, $\varphi(t)$ is the fraction of water loss for evaporation and infiltration. Substituting (6) into (8), we obtain a closed equation of storage dynamics in the catchment scale

$$\frac{dh}{dt} = p(t) - kh^d. \qquad (9)$$

In a steady state $dh/dt = p - kh^d = 0$ and $h = (p/k)^{1/d}$. Further we will mark steady-state quantities by index 0 and perturbations by index 1. In this notation $h_0 = (p_0/k)^{1/d}$. Represent p and h as

$$p(t) = p_0 + p_1(t), \quad h(t) = h_0 + h_1(t). \tag{10}$$

At small perturbations $|p_1| << p_0$, $|h_1| << h_0$ equation (9) can be linearized

$$\frac{dh_1}{dt} = p_1(t) - \kappa h_1, \tag{11}$$

where we introduced the decay constant

$$\kappa = dkh_0^{d-1} = dk^{1/d} p_0^{1-1/d}, \tag{12}$$

which depends both on catchment characteristics (via k and d) and on the effective precipitation (via p_0).

It is difficult to say somewhat about the random process $p_1(t)$, but we can draw some information on it from its Fourier spectrum that is considered below.

2.4. Storage and runoff power spectra

The Fourier transform of equation (11) has the form

$$i\omega H(\omega) = P(\omega) - \kappa H(\omega), \tag{13}$$

where

$$H(\omega) = \int_{-\infty}^{\infty} h_1(t) e^{-i\omega t} dt, \quad P(\omega) = \int_{-\infty}^{\infty} p_1(t) e^{-i\omega t} dt.$$

It follows from (13) that

$$H(\omega) = \frac{P(\omega)}{\kappa + i\omega}. \tag{14}$$

Based on (14) one can find the correlation function spectral density (also called the power spectrum) of water storage:

$$S(\omega) = |H(\omega)|^2 = \frac{|P(\omega)|^2}{\kappa^2 + \omega^2}. \tag{15}$$

The power spectrum of precipitates includes delta-like responses on periodic processes and a multiplicative noise distributed by a power law:

$$|P(\omega)|^2 = \sum_{n \geq 1} B_n |\omega|^{-\beta} [\delta(\omega - \omega_n) + \delta(\omega + \omega_n)], \tag{16}$$

where n is a spectral component number, ω_1 is the base frequency corresponding to annual periodicity of synoptic processes, $\omega_n = n\omega_1$ are the multiple frequencies, B_n are the amplitudes of corresponding responses.

The correlation function of storage has annual periodicity with decay because of the loss of information on details of the random process in averaging by an ensemble of realizations. It is known that the decay of an oscillating correlation function leads to widening delta-like peaks in its spectrum. Instead of infinitely high peaks with zero width $\delta(\omega \pm \omega_n)$, we obtain finite peaks $\delta(\omega \pm \omega_n, \varepsilon_n)$ with a width ε_n and a height $1/\varepsilon_n$. The form of the finite peaks is described by the function

$$\delta(x, \varepsilon) = \frac{\pi^{-1}\varepsilon}{\varepsilon^2 + x^2},$$

which tends to $\delta(x)$ in the limit $\varepsilon \to 0$.

Substitution of (16) into (15) with regard to the finiteness of ε_n yields

$$S(\omega) = \frac{|\omega|^{-\beta}}{\kappa^2 + \omega^2} \sum_{n \geq 1} B_n [\delta(\omega - \omega_n, \varepsilon_n) + \delta(\omega + \omega_n, \varepsilon_n)]. \qquad (17)$$

Thus, the power spectrum of water storage decays as $\sim |\omega|^{-\beta}$ at low frequencies $|\omega| < \kappa$ and as $\sim |\omega|^{-\beta-2}$ at high frequencies $|\omega| > \kappa$. The change of behavior occurs at the crossover point $|\omega| = \kappa$.

Based on (17) it is easy to find the runoff power spectrum. Separation of the total runoff on a steady-state part and a perturbation yields $q(t) = q_0 + q_1(t)$. Using (6) and (10), we get

$q_0 = kh_0^d = p_0, \quad q_1 = \kappa h_1$.

The spectral form of the last equation is

$Q(\omega) = \kappa H(\omega)$,

where

$$Q(\omega) = \int_{-\infty}^{\infty} q_1(t) e^{-i\omega t} dt$$

is the Fourier transform of $q_1(t)$. Hence, within this approximation the runoff power spectrum $|Q(\omega)|^2$ differs from the storage spectrum (17) only by the constant multiplier κ^2. Introducing a redefined parameter B_n as the former B_n multiplied by κ^2, i.e. $B_n^{\text{new}} = \kappa^2 B_n$, we can use again the same formula (17) for the runoff power spectrum.

Considering power spectrum (17), we can separate it into three multipliers. The first of them is the sum of spectral components at the annual frequency and its harmonics. The second multiplier

is a continuous 1/*f*-noise, namely $1/f^{\beta}$ with the exponent $\beta \sim 1$. Finally, the third multiplier is the Lorentzian $(f_c^2 + f^2)^{-1}$. Here we have introduced the frequency $f = \omega/2\pi$ and a modified damping constant (or crossover frequency) $f_c = \kappa/2\pi$ corresponding to the decay constant κ. If f is small compared to f_c, the 1/*f*-noise specifies behavior of the spectrum. But when f passes through the point f_c, the Lorentzian transforms into f^{-2} and, being multiplied by $1/f^{\beta}$, it yields a trend of $1/f^{\beta+2}$ at high frequencies.

3. Case studies

3.1. Catchment characteristics

Now we apply the above theoretical relationships to the analysis of daily water discharges of the rivers Volga at Staritsa, Tvertsa at Mednoe, Tma at Novinki, and Moskva at Rublevo. Time series of river discharges were obtained from the databases of the Russian Federation Hydrometeorology Committee (for the Volga, Tvertsa and Tma) and the municipal enterprise on water supply and wastewater treatment "Mosvodokanal" (for the Moskva) (Dolgonosov et al., 2004). A schematic map of the river catchments is displayed on Fig. 1. Table 2 presents some catchment characteristics and statistical parameters of the daily river discharge time series.

Power spectra were calculated on the basis of the standard Fourier analysis procedure. As Rao and Hamed (2003) wrote, raw spectra suffer from large variances; therefore several smoothing techniques are proposed to reduce this drawback (Priestley, 1984). Such smoothing usually involves different types of spectral averaging windows, though this procedure often results in poor spectral resolution. Another problem is the spectral window leakage (Percival and Walden, 1993) that causes disbalance of the power at different frequencies, thus making it difficult to isolate different spectral components. The power leakage can be reduced by using specialized windows but again at the expense of spectral resolution.

In our calculations we used the Tukey–Hamming window (Marple, 1987) that partially neutralizes the effect of throbbing between harmonics of the given time interval and eigenfrequencies of the process. This window offers good compromise between widening of spectral components and distortion of their lateral parts.

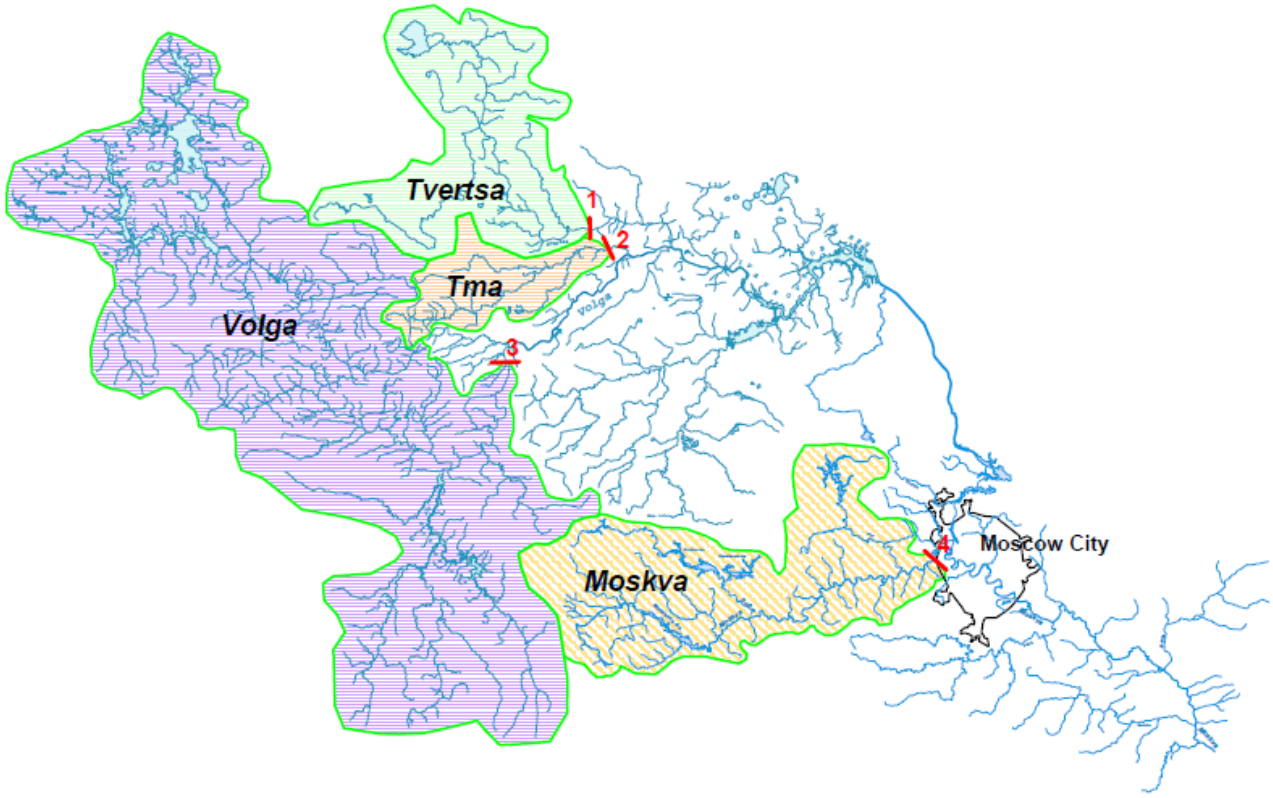

Fig. 1. Map of the river catchments under study: 1 – Tvertsa at Mednoe; 2 – Tma at Novinki; 3 – Volga at Staritsa; and 4 – Moskva at Rublevo (designed by A.A. Artemiev).

Table 2. General characteristics of the rivers and their daily discharge time series

River and gauging station	Catchment area, km^2	Observation interval, years (days)	Daily river discharge, m^3/s mean min÷max	Standard deviation, m^3/s	Skewness	Kurtosis
Volga at Staritsa	21100	1979–1996 (6575)	170 26.4÷1780	171	3.48	17.6
Moskva at Rublevo	7530	1994–2003 (3580)	20.8 1÷748	33.8	12.1	207
Tvertsa at Mednoe	6510	1979–1996 (6575)	73.8 1.8÷1220	71.0	3.51	22.4
Tma at Novinki	1850	1980–1996 (6210)	13.0 2.1÷950	22.4	14.7	507

The calculated power spectra of river discharges are plotted on Fig. 2 in double logarithmic coordinates. The frequency f varies within a range of 10^{-3} day^{-1} up to the Nyquist limit $f_N = 1/(2\Delta T)$, which in this case is equal to 0.5 day^{-1} because the time step of water discharge series is $\Delta T = 1$ day. The dimension of power spectral density is equal to the squared dimension of water discharge multiplied by the time step dimension, i.e. $[S] = (\text{m}^3/\text{s})^2$ day.

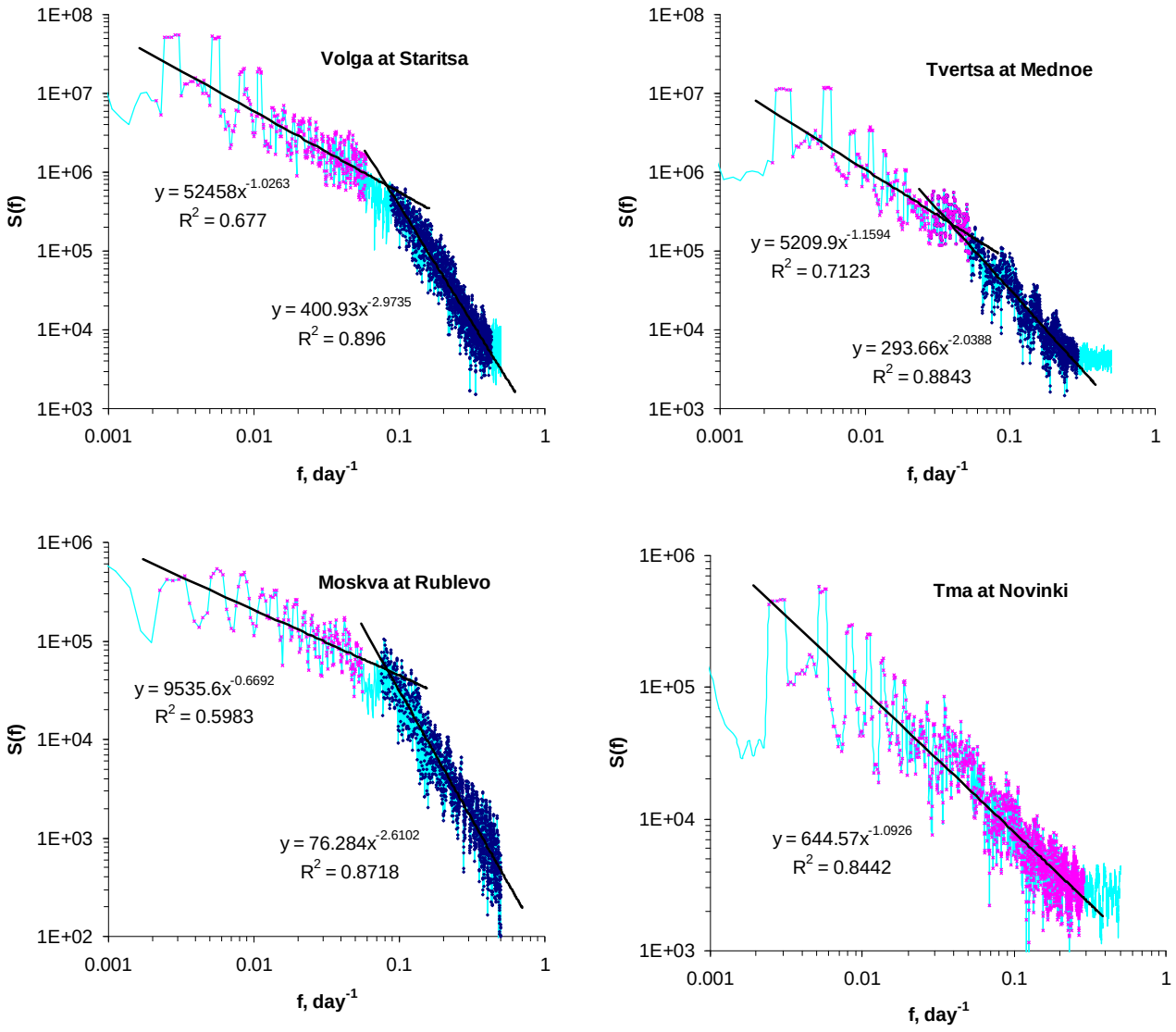

Fig. 2. Power spectra of river discharge time series.

The spectra on Fig. 2 exhibit their main component at the annual frequency $f_1 = (1/365.25)$ day^{-1} and harmonics at multiple frequencies $2f_1, 3f_1$, etc. Almost all the spectra (excluding one for the river Tma) show two regions of different trends. The trends can be described by a power-law regression

$$S = Bf^{-b} \qquad (18)$$

depicted on Fig. 2 (see also Table 3). The determination coefficient R^2 varies from 0.6 to 0.9.

Table 3. Crossover frequency and characteristics of power-law trends in different spectral regions

River	Exponent b		Crossover frequency f_c, day^{-1}
	Low frequency region	High frequency region	
Volga at Staritsa	1.026	2.974	0.0834
Moskva at Rublevo	0.669	2.610	0.0810
Tvertsa at Mednoe	1.159	2.039	0.08 ± 0.02
Tma at Novinki	1.093	–	~0.3

A spectral trend with density $S \sim f^{-b}$ at $b > 0$ describes the influence of noise. The particular case at $b \sim 1$ is usually called the 1/*f*-noise (Kuzovlev and Bochkov, 1982; Schroeder, 1991; Lowen and Teich, 1993; Vladimirov et al., 2000). It is seen from Table 3 that the noise component of river discharge spectra at low frequencies is just referred to the type of 1/*f*-noise. The jump of the exponent b at transition to high frequencies is caused by the resistance of water flow on catchment, which damps high frequency oscillations of river runoff.

In log–log coordinates the power-law dependence (18) looks like a straight line with slope $-b$. At low frequencies the exponent b is close to 1 for the rivers Volga, Tvertsa and Tma, whereas it is equal to 0.67 for the Moskva. After transition into high frequencies, this exponent rises by ~2 for the Volga and Moskva, only by ~1 for the Tvertsa, and does not change at all for the Tma. The crossover between the two spectral regions for the Volga and Moskva lies at the frequency $f_c \approx 0.08$ day^{-1} that corresponds to a period of $\tau_c = 1/f_c \approx$ 12 days. At low frequencies there are 30 spectral components between the annual peak and the crossover. At high frequencies, spectral components are not resolved and spectrum becomes continuous. For the Tvertsa, the crossover lies somewhere within the frequency range 0.06 – 0.10 day^{-1}, but it is difficult to localize it because the transition is very diffuse. For the Tma, the crossover takes place out of the observed range of frequencies, at least at a frequency of ~0.3 day^{-1}.

The high frequency spectral region describes short-term variations of river flow lasting much less than 12 days that is typical for weak rainfalls. The low frequency region describes long-term variations of river flow with periods much more than 12 days that can be caused by large-scale seasonal phenomena such as spring tide due to snowmelt lasting about a month, long autumn rainfalls, and summer and winter low-water periods.

3.2. Estimation of model parameters

The empirical spectra were approximated by formula (17). The parameter β in (17) corresponds to the low frequency values of the empirical exponent b present in Table 3. The parameter κ can be found as $2\pi f_c$. The parameters ε_n and B_n were estimated separately for each of the first seven peaks and then corrected taking into account superposition of peaks. Values of these parameters for farther peaks were adopted the same as for the seventh one. The results obtained are present in Table 4. Instead of the parameter B_n having a fractional dimension we introduce a quantity

$C_n = B_n \omega_1^{-\beta-1}$

(where $\omega_1 = 2\pi f_1 = 0.01720$ rad/day), which has the same dimension as the power spectral density $|Q(\omega)|^2$ of river runoff.

Table 4. Parameters of river runoff power spectra (ε_n, rad/day; C_n, 10^6 $(m^3/s)^2$ day)

n	Volga at Staritsa		Moskva at Rublevo		Tvertsa at Mednoe		Tma at Novinki	
	ε_n	C_n	ε_n	C_n	ε_n	C_n	ε_n	C_n
1	0.2	5.64	0.4	0.0749	0.2	1.07	0.2	0.689
2	0.2	11.3	0.4	0.145	0.2	2.52	0.2	1.58
3	0.2	7.52	0.4	0.176	0.2	1.16	0.2	1.23
4	0.2	9.40	0.4	0.159	0.2	1.81	0.2	1.48
5	0.2	5.64	0.4	0.159	0.2	1.29	0.2	1.23
6	0.3	7.52	0.4	0.132	0.3	1.29	0.3	1.53
$n \geq 7$	0.3	7.52	0.4	0.132	0.3	1.29	0.3	1.48

Table 4 shows that the rivers Volga, Tvertsa and Tma have the same values of the parameter ε_n. This can be explained by the fact that their catchments are situated close to each other (see Fig. 1) so that rainfalls on these territories strongly correlate. For the river Moskva the width of spectral peaks are a little larger than that of the other rivers ($\varepsilon_n = 0.4$ against $\varepsilon_n = 0.2$ and 0.3 rad/day) (this is also clear from Fig. 2). The larger is the width ε_n of spectral peaks, the shorter will be the correlation time τ_n as it follows from the relationship $\tau_n = 2\pi/\varepsilon_n$. In particular, values of ε_n = 0.2, 0.3 and 0.4 rad/day yield correlation times τ_n = 31, 21 and 16 days respectively.

3.3. Comparison of model and empirical power spectra

The model and empirical spectra of river runoffs are depicted on Figs. 3–6.

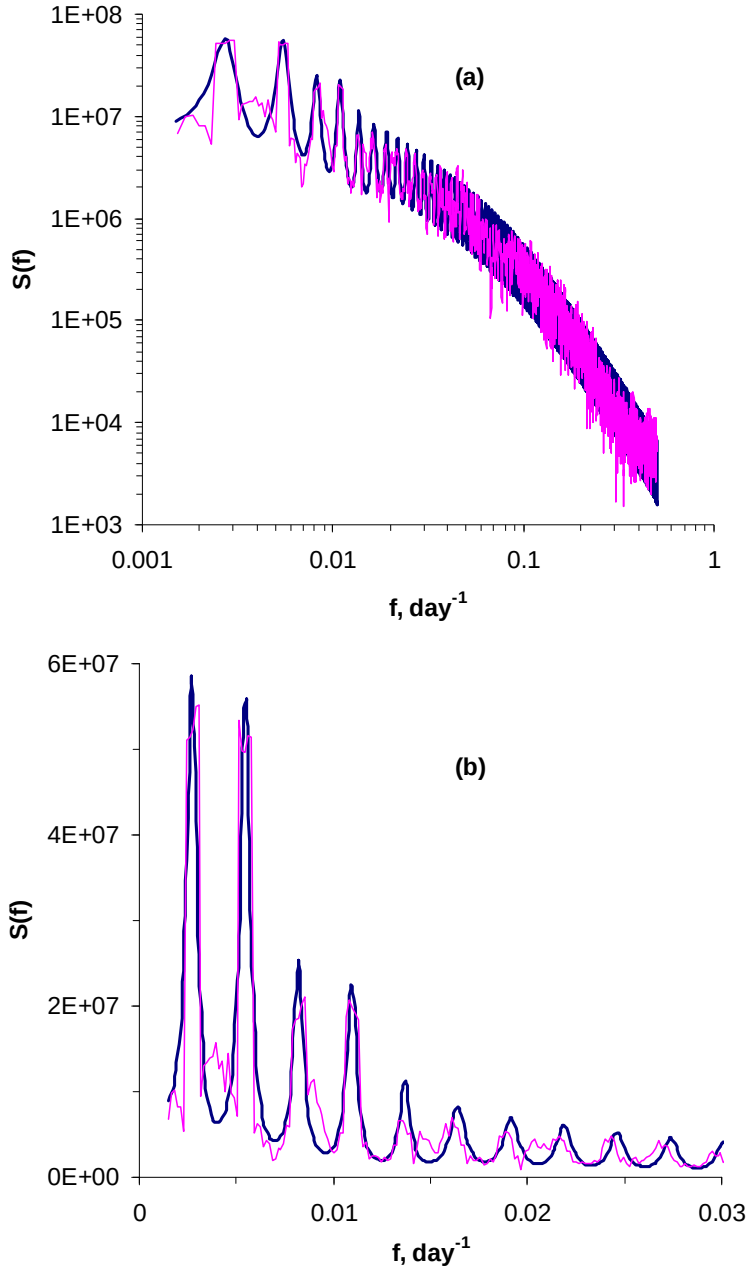

Fig. 3. River Volga at Staritsa: model (bold curves) and empirical (thin curves) power spectra: (a) throughout the range of observed frequencies in log–log coordinates; (b) first 10 peaks in linear coordinates.

Consider the Volga power spectrum in Fig. 3. The upper plot (Fig. 3a) covers the entire power spectrum in log–log coordinates and the lower plot (Fig. 3b) shows the first ten peaks in linear coordinates. The spectrum begins from the peak at the annual frequency f_1. Then peaks at multiple frequencies follow and the spectrum gradually turn from a discrete into a continuous form.

The model spectrum is in good agreement with the empirical one. One can see a smooth transition between low and high frequencies in the crossover zone in accordance with the empirical spectrum. The lower plot shows striking coincidence of the first several peaks, but farther empirical peaks shift a little towards lower frequencies.

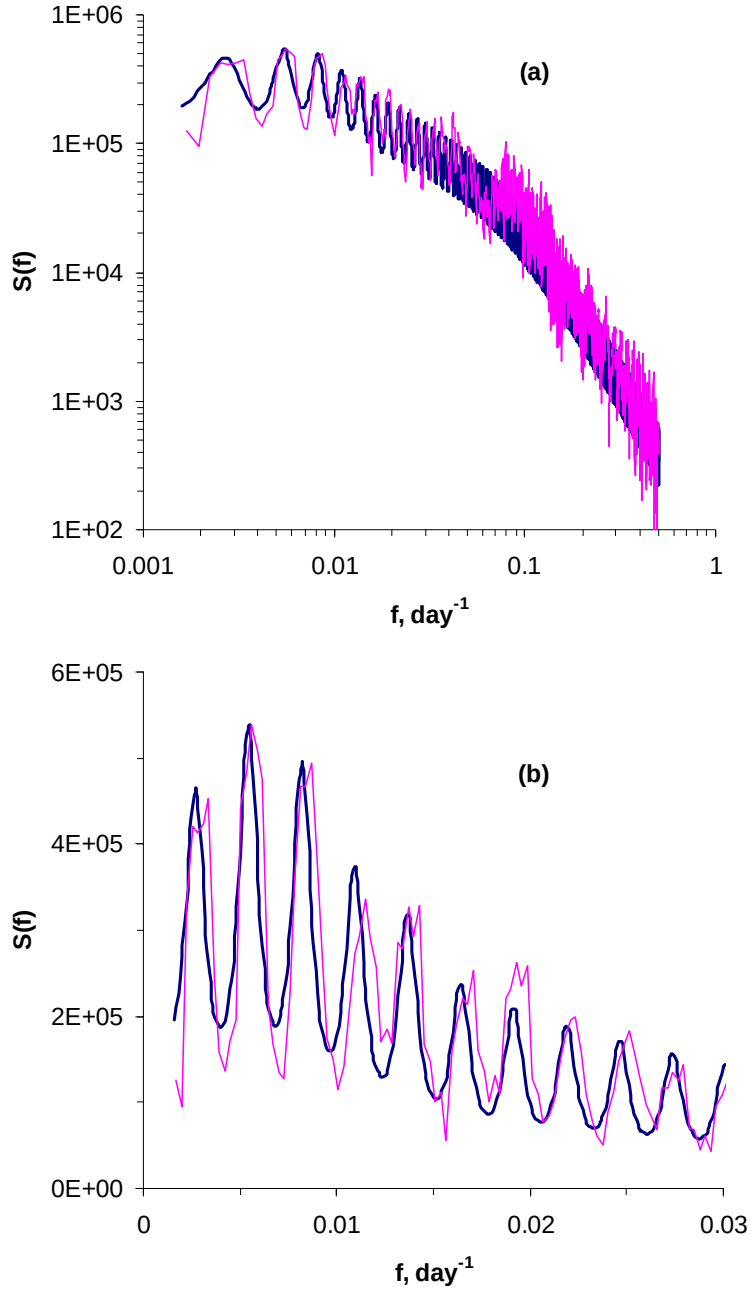

Fig. 4. River Moskva at Rublevo (cf. Fig. 3).

The river Moskva spectra (Fig. 4) are also in agreement but not so good as for the Volga. In the region of discrete spectrum (low frequencies, Fig. 4b) there is a systematic deviation of the right-hand slopes of empirical peaks from the model curve. In the high frequency region, the oscillations of empirical spectrum occur with the amplitude slightly exceeding that of model spectrum. But in the crossover zone (frequencies 0.05 – 0.1 day^{-1}) the empirical spectrum is highly

irregular and goes noticeably out of the bounds of model spectrum. Nevertheless, there is qualitative agreement between the model and empirical spectra.

At high frequencies the river Tvertsa power spectrum (Fig. 5) has a white-noise tail with uniformly distributed spectral density at frequencies above 0.2 day^{-1} that corresponds to periods less than 5 days (Fig. 5a). However, as noticed by Feng et al. (2004), the white noise is probably an artifact caused by heterogeneous of time series and maybe by relatively large contribution of errors into low-amplitude, short-period oscillations of runoff. Except for the white-noise tail, the whole empirical spectrum lies within the amplitude of oscillations of the model spectrum; noticeable overshootings happen seldom enough. At low frequencies the first seven peaks coincide well, but farther the empirical spectrum behaves less regular.

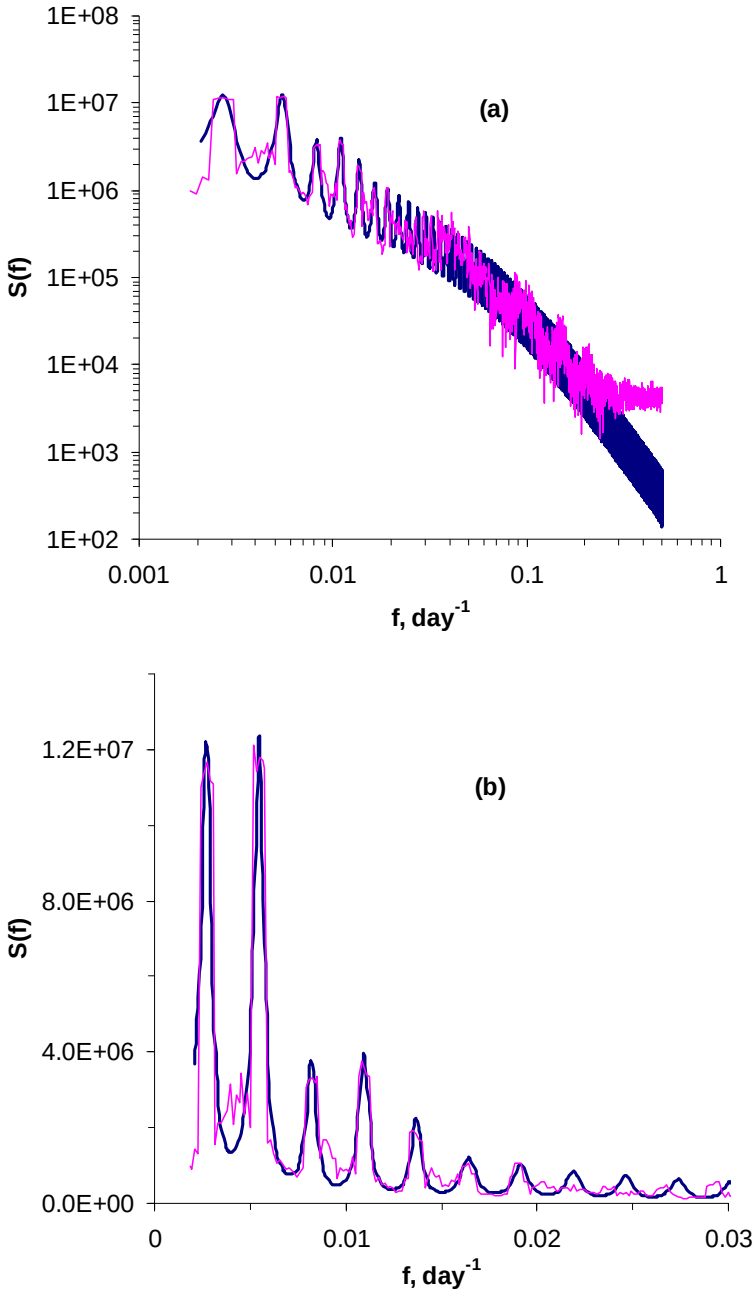

Fig. 5. River Tvertsa at Mednoe (cf. Fig. 3).

The river Tma power spectrum also has a similar white noise tail at $f > 0.2$ day^{-1} (Fig. 6a) of the same origin as above. Except for this tail, there is satisfactory agreement at high frequencies. In the low frequency region (Fig. 6b) the first seven peaks show good congruence, but farther the empirical spectrum strongly fluctuates.

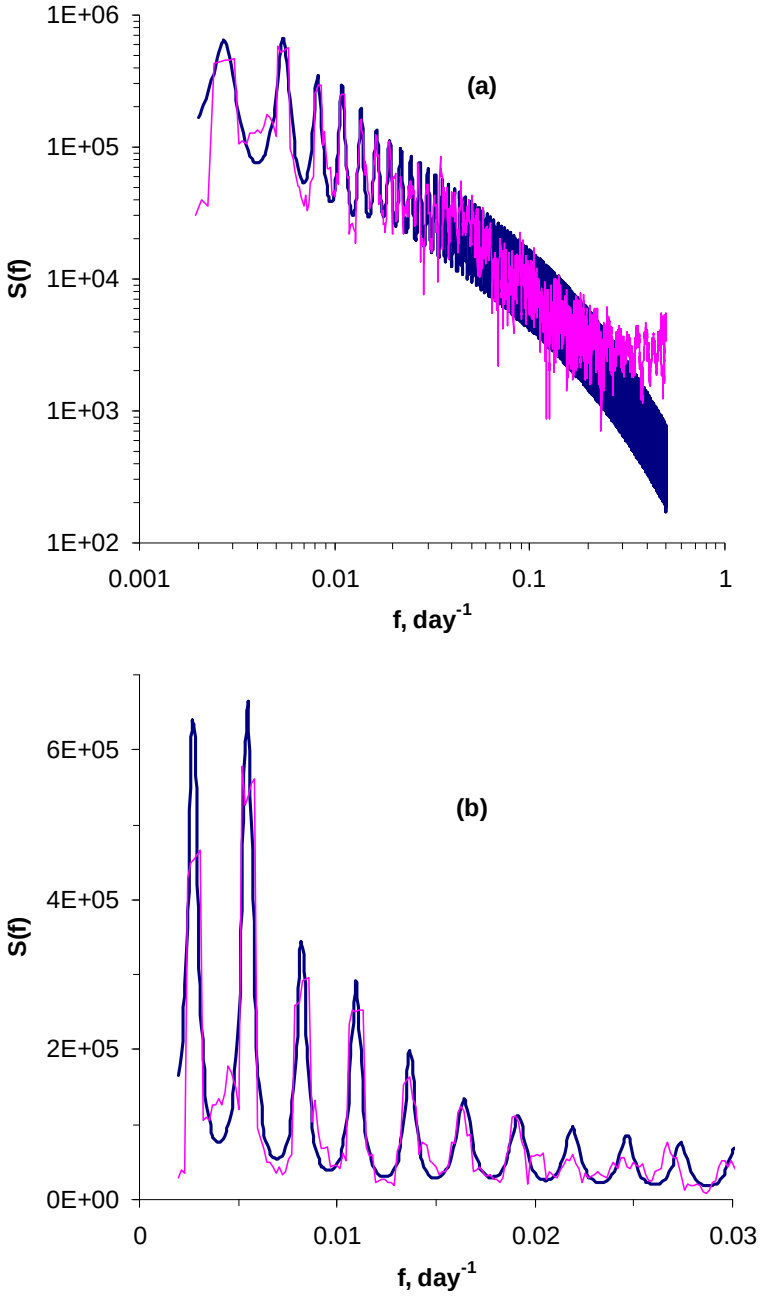

Fig. 6. River Tma at Novinki (cf. Fig. 3).

Thus, the obtained expression (17) for power spectral density satisfactory describes river runoff spectra.

Generally, comparing the theoretical results with observation data, it is necessary to distinct two alternative ways of data treatment: 1) based on empirical regressions in the form of power law $S \sim f^{-b}$ and 2) based on the theoretical formula including not only a 1/*f*-noise term, but also the Lorentzian damping as well as the contribution of annual oscillations and their harmonics. Fig. 2 shows results of the first way of treatment, without using the theoretical formula. The fact that on Figs. 2c,d the apparent break of trend slope less than 2 suggests only that empirical regressions do not always reflect reality. This may be caused for example by deficiency of data or their inaccuracy. Actually, treatment of the same data using the derived formula shows (see Fig. 5) that the theoretical dependence quite adequately describes the transformation of the spectrum at moving towards high frequencies. Some discrepancies, especially the appearance of a white-noise tail, can be caused mainly by data scattering, non-equidistant measurements (in view of gaps in the data), distortions in the calculation of empirical spectra from time series using the Tukey-Hamming smoothing procedure, enlarged relative errors in the measurements of high-frequency runoff oscillations. The same takes place for Fig. 6, where the high-frequency spectral region is merely moved beyond the Nyquist limit. Therefore we cannot observe the theoretically predicted break of trend slope in this case. The theory can correct very inexact empirical spectra and suggests what we could observe having more accurate data. In any case, validation of the model should be continued based on more qualitative information.

3.4. Crossover frequency

Low and high frequency trends obey power laws. In particular, at low frequencies there occurs a 1/*f*-noise imposed on the regular peak of annual periodicity and its harmonics. As the general analysis shows, there is a crossover between low and high frequency trends with changing the exponent of 1/*f*-noise by two units, i.e. $S \sim f^{-\beta}$ transits into $S \sim f^{-\beta-2}$ with growing frequency. The seeming violation of this theoretical conclusion for empirical spectral trends of the rivers Tvertsa and Tma (Figs. 2c,d) (remember that in the former case the noise exponent changes only by ~1 and in the latter one this crossover is not observed at all) is caused, on the one hand, by strong data scattering and, on the other hand, by shorter part of the Tvertsa time series at high frequencies and complete missing of this spectral region in the observed frequency range for the Tma.

The crossover period

$$\tau_c = 1/f_c = 2\pi/\kappa = 2\pi/(dk^{1/d} p_0^{1-1/d})$$

(see (12)) depends on the mean precipitation p_0 and also, via the parameters k and d, on dissipative processes during runoff formation, which damp high frequency runoff oscillations at

$f > f_c$.

The quantity τ_c characterizes a time scale of runoff formation on catchment. It depends generally both upon the travel time τ_t of water through catchment and upon the rainfall duration τ_r. Travel times are crucial for the runoff formation on small catchments where these times are usually less than the typical rainfall duration. However, rainfall durations are more important for large catchments where they are less than the total travel time. This reasoning can be reproduced, in outline, by an interpolation formula

$\tau_c^{-1} = \tau_t^{-1} + \tau_r^{-1}$.

Travel time depends on the catchment length L as $\tau_t = L/u$, where u is a characteristic speed of water flow in the river network. Rainfall duration is a constant (on average) for a given territory, but generally depends on geographic location and climate change. At the crossover, travel time coincides with rainfall duration: $\tau_t = \tau_r$ or $L/u = \tau_r$, that yields a spatial scale $L_r = u\tau_r$ where runoff processes on catchment correlate. If catchment length is larger than this scale $L > L_r$, the catchment embraces remote uncorrelated parts. In this case $\tau_t > \tau_r$ and hence $\tau_c \approx \tau_r$. It implies that for large catchments with synoptically-unconnected parts the crossover period τ_c (and crossover frequency f_c) remains constant independently of catchment length. On the contrary, at small catchment length $L < L_r$ typical rainfalls cover the entire catchment area. In this case $\tau_t < \tau_r$ that leads to $\tau_c \approx \tau_t = L/u$, i.e. the crossover period is proportional and the crossover frequency is inversely proportional to the catchment length. Hence, with decreasing catchment length the crossover point f_c will move towards high frequencies.

Water discharge through the closing site can be found by summing contributions of all catchment parts with regard to their travel times (Spitsyn and Sokolova, 1990). Rapid, small-scale processes on catchment little contribute to the total discharge. This results in the damping of high frequency oscillations in runoff power spectra. At the same time, slow, large-scale processes prevail in the total river discharge. That is why the trends of runoff power spectra have different slopes in different spectral regions.

The break in trend slope has been noted earlier by Radziejewski and Kundzewicz (1997) and Pandey et al. (1998). Pandey et al. (1998) obtained an integrated power spectrum using normalized daily river flow time series for 19 US river basins with catchment areas from 5 km^2 to 2 million km^2 and mean water discharges from 0.1 to 5000 m^3/s. Spectral trends were approximated by power-law dependence (18). At low frequencies ($10^{-4} - 10^{-1}$ day^{-1}; respective periods 14 years to 10 days) the spectral trend is characterized by the exponent $b = 0.72 \pm 0.30$ averaged by the ensemble of rivers.

At high frequencies (0.1 – 0.5 day^{-1}; periods 10 to 2 days) the trend has $b \approx 2.47$. These values are in qualitative agreement with our results represented in Table 3.

As mentioned above, spectral trends have a crossover. The crossover period is 12 days for the rivers Volga, Moskva and Tvertsa and decreases to ~3 days for the Tma. Dahlstedt and Jensen (2003) studying the Mississippi sites found that all of them have approximately the same spectrum, which consists of two power-law regimes separated by a period of 20 to 40 days. At low frequencies the power-law exponent is close to −1 corresponding to logarithmic decaying correlations in the long time limit (Jensen, 1998), but at high frequencies this exponent is close to −3 that is in agreement with our results. For the Danube the crossover depends on basin area with periods equal approximately to 10 days for Dilligen and Ingolstadt (basin areas 11315 and 20001 km^2 respectively), 20 days for Nagymaros (183534 km^2), and 60 days for Orsova and Ceatal Izmail (576232 and 807000 km^2). These data can be described roughly by a dependence of $\tau_c = 0.07L$, where $L = \sqrt{A}$ is the catchment length (in km) and τ_c is the crossover period (in days) (Fig. 7). The period of 12 days found in our work for the Volga, Moskva and Tvertsa with catchment areas of 6500 to 21000 km^2 and the period of ~3 days for the Tma (1850 km^2) are also indicated on this figure for comparison.

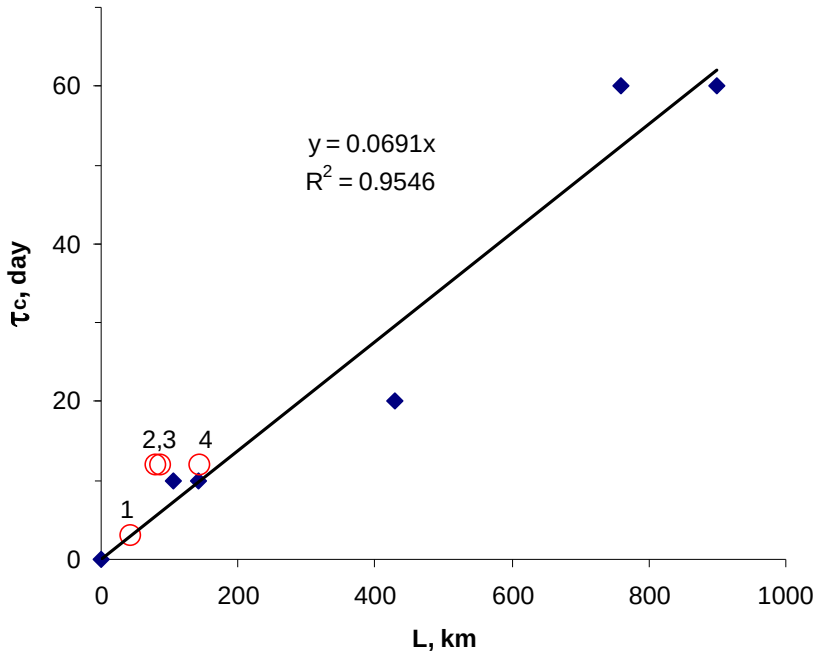

Fig. 7. Crossover period versus catchment length for a series of the Danube catchments. Special markers indicate values for the rivers Tma (1), Tvertsa (2), Moskva (3), and Volga (4).

In contrast to Dahlstedt and Jensen (2003), Pandey et al. (1998) considered data from different sites and rivers as realizations of the same process and the power spectra were averaged over all sites. That is why there are generally no references to how the crossover point changes with basin area.

Pandey et al. (1998) also found that the crossover period varies from 3 to 24 days with an average of 6 days. Tessier et al. (1996) obtained the range of periods from 10 to 30 days with an average of 14 days. These periods are typical for lifetimes of global atmospheric synoptic structures (Koloshnikova and Monin, 1965). On this basis, Tessier et al. (1996) and then Pandey et al. (1998) supposed that the crossover itself is caused by these structures. As mentioned above, theoretically such a situation takes place only for large catchments, but for small one the crossover period is determined by the travel time of water through catchment rather than by the rainfall duration.

3.5. Runoff fluctuations power spectra

Along with the calculation of power spectrum directly, using time series of discharges as done by Tessier et al. (1996) and Pandey et al. (1998), another approach to data processing based on the preliminary isolation of trend can be used. This approach was realized by Pelletier and Turcotte (1997), who subtracted trend values, determined as the multiyear average discharge for every month, from monthly river discharge time series. The series detrended in that way describes fluctuations of water discharges. Calculations showed that the fluctuation power spectrum can be approximated again by power law (18) but with the exponent b close to 0.5. It was also shown that the model of random walk on a one-dimensional lattice of 32 sites with periodic boundary conditions gives similar exponent value. Earlier Scher et al. (2002) have shown that a continuous-time random-walk model also can produce the $1/f$ scaling of spectrum. Because Pelletier and Turcotte (1997) operated with monthly data, high frequency asymptotics remained beyond their scope. Therefore, the above-mentioned crossover between low and high frequency asymptotics was not revealed in the stated work.

To obtain fluctuation spectrum for the rivers under study and compare our results with data of Pelletier and Turcotte (1997), we conducted additional calculations with detrended time series of river discharges. The trend is determined as a multiyear average discharge on every date of a year. This averaged daily hydrograph for the Volga at Staritsa is displayed on Fig. 8a. Power spectrum of this hydrograph and its power-law approximation are depicted on Fig. 8b. The detrended time series of discharge fluctuations was used to calculate the fluctuation power spectrum (Fig. 8c).

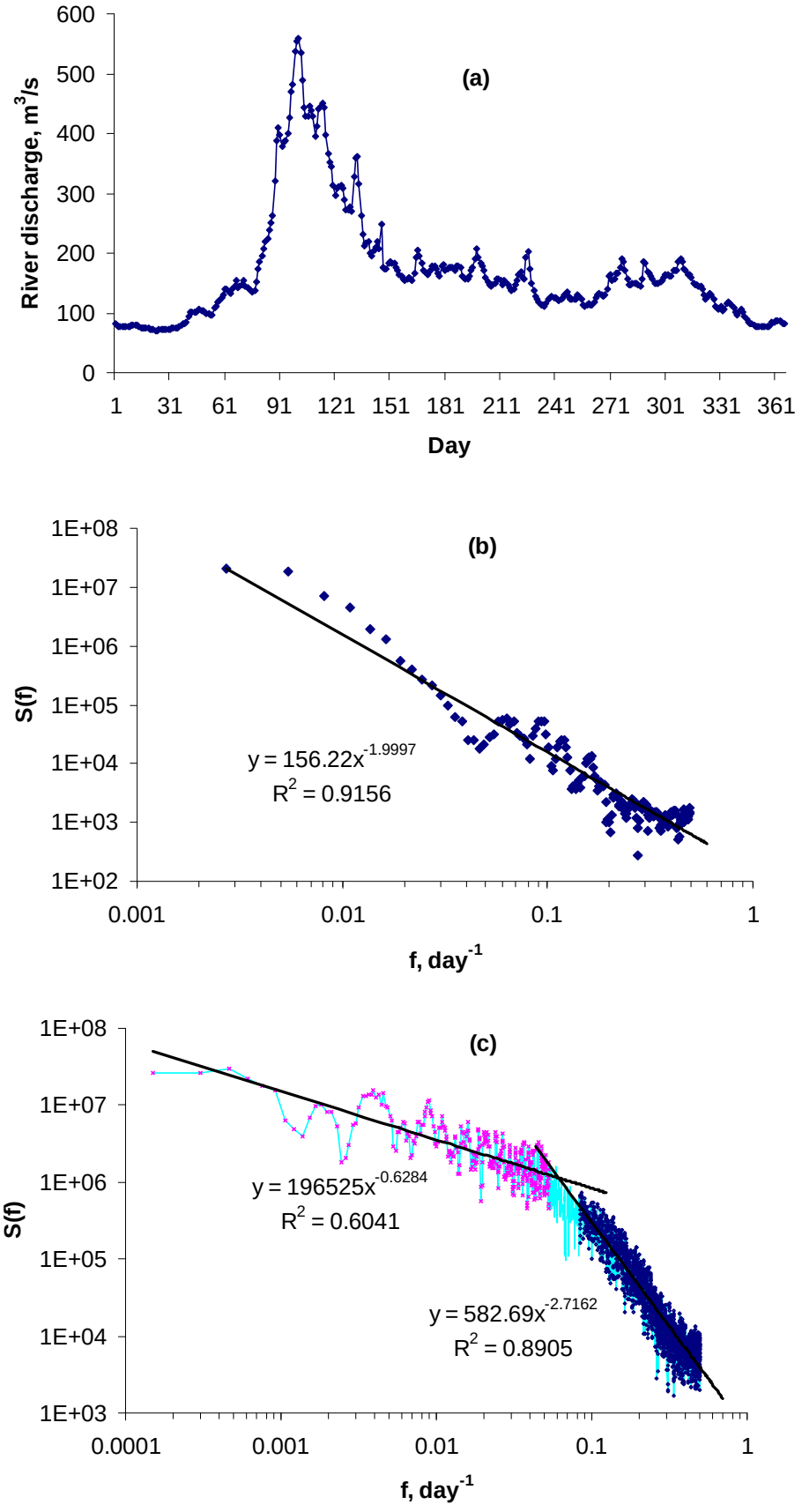

Fig. 8. (a) Multiyear-averaged time series of daily discharges of the river Volga at Staritsa during a year; (b) power spectrum of the averaged time series; and (c) fluctuation power spectrum.

This spectrum, like the power spectrum of raw (not detrended) time series, has two different power-law asymptotics like (18): with the exponent $b \approx 0.6$ in the low frequency region and $b \approx 2.7$ in the high frequency one. The exponent values differ by about 2 as before the isolation of trend (cf. Fig. 2), but the crossover frequency slightly moves to a value corresponding to a period of 15 days (instead of 12 days). The low frequency exponent ~0.6 is close enough to the value ~0.5 obtained by Pelletier and Turcotte (1997) using monthly data and confirmed by the random walk model.

4. Conclusions

The main result of the work consists in the deduction of the analytical expression for water runoff and storage power spectra and in their application to draw information on catchment characteristics from river discharge time series. We developed integrated runoff and storage dynamics without detailing of catchment structure that allowed revealing the generalized reaction of the whole catchment on an external impact. In this approach all features of the catchment such as the structure of river network, the presence of lakes and reservoirs, precipitation characteristics, etc., are implicitly included into the model parameters; this is a typical situation for a phenomenological theory.

For better understanding of a coupling between the water runoff q and the storage h we deduced dynamic equations, analyzed relaxation times for runoff and storage, and showed that h is a slow variable (i.e. an order parameter) and q is a fast variable, which follows a slow change of h. As numerical estimation indicated, q reaches its local equilibrium state for a short time measured by minutes, whereas h changes for a much longer time measured at least by days. This feature allowed us to simplify one of the dynamic equations (following the synergetic subordination principle) and to obtain a scaling relationship of $q = kh^d$ with parameters k and d independent of time. This relationship is not an empirical approximation but a theoretically derived result. We cannot arbitrarily accept a simpler linear relationship between q and h that sometimes happened in the literature, because it does not reflect physical reasons.

The nonlinear dynamic equations derived for runoff and storage were linearized in the neighborhood of a steady state. The linearized storage equation was transformed into the spectral form binding the storage spectrum with the precipitation one. The precipitation power spectrum was represented as the sum of the decaying periodic components multiplied by the noise frequency factor $1/f^{\beta}$ with the exponent $\beta \sim 1$. It was shown that the storage power spectrum is the product

of the precipitation power spectrum and the Lorentzian $(f_c^2 + f^2)^{-1}$. The same form has the runoff power spectrum differing only by a constant factor.

Below the characteristic frequency f_c the Lorentzian is nearly constant and therefore the trend of runoff power spectrum at low frequencies is determined by the noise $1/f^{\beta}$. However, above this frequency the Lorentzian transforms into f^{-2} and with the stated noise it yields the combined trend $1/f^{\beta+2}$ at high frequencies.

The theoretical formula derived for runoff power spectrum describes annual oscillations and their harmonics and therefore inevitably must include amplitudes and widths of spectral modes. An attempt to decrease the number of model parameters by excluding the amplitudes and widths is equivalent to exclusion of these spectral modes from the model at all. Obviously, such a model will not be able to analyze annual and intra-annual runoff oscillations. This essentially impoverishes the theory remaining only the 1/*f*-noise trend and the Lorentzian term in the power spectrum formula. Meanwhile, the analysis of the derived formula shows that each separate factor in it correctly describes empirical spectra: 1) the presence of power-law trend confirms the existence of 1/*f*-noise; 2) the break of trend slope at transition into high frequencies clearly demonstrates the action of the Lorentzian damping; 3) spectral peaks are situated close to their theoretical positions. Thus the theory gives a qualitatively correct description of the observed spectral behavior. As to calculation of the amplitudes and widths of spectral modes, the developed theory certainly does not allow doing this. For this purpose it is necessary to find dependencies of these parameters on precipitation and catchment characteristics. However, this is another problem lying out of the scope of our article.

The theoretical relationships were applied to river discharge time series. The case studies were carried out for the river Volga at Staritsa and three more rivers of the Volga basin: the Moskva at Rublevo, the Tvertsa at Mednoe, and the Tma at Novinki, with catchment areas of 1850 to 21100 km^2. The time series were used to calculate empirical power spectra of river discharges and to construct model power spectra by fitting model parameters to the data. The calculations have shown that the model and empirical spectra are in good agreement, especially total trends and first several components. All the spectra have discrete components superimposed on a continuous background of fluctuations. With increasing frequency the spectra turn gradually from a discrete into a continuous form. Two spectral regions with different slopes of the power-law trends can be separated. In the crossover zone there is a smooth transition between the two regions. The crossover corresponds to a period of 12 days for large catchment areas and of ~3 days for small one. The high frequency region is typical for weak rainfalls, which generate short-term variations of river flow lasting less than the crossover period. The low frequency region describes long-term variations of river flow with periods more than the crossover one. These variations can be provoked by large-

scale seasonal phenomena such as spring tide, long autumn rainfalls, and summer and winter low-water periods.

The crossover period depends generally both on travel time of water through catchment and on rainfall duration. Travel time is crucial for small catchments, and rainfall duration for large one. Travel time is inversely proportional to catchment length; by this cause the crossover shifts towards small periods (or high frequencies) with decreasing catchment length. Since rainfall duration is independent of catchment area, the crossover period for large synoptically-unconnected catchments remains constant. River discharge through the closing site can be found by summing contributions of all catchment parts with regard to their travel times. Rapid, small-scale processes on catchment little contribute to the total discharge. This results in the damping of high frequency oscillations in runoff power spectra. At the same time, slow, large-scale processes dominate in the total river discharge. All these conclusions are confirmed by the empirical runoff power spectra.

Additional calculations to obtain a detrended time series of river discharges were carried out for studying fluctuations. The trend was determined as a multiyear average discharge on every date of a year. The fluctuation time series detrended in such a way was used to calculate the fluctuation power spectrum. This spectrum has two different power-law asymptotics differing in their exponents by about 2 units like the power spectrum of original (not detrended) time series in agreement with our theoretical results.

Acknowledgements

We are gratefully acknowledged to A.A. Artemiev (Institute of Water Problems, Russian Academy of Sciences) for elaboration of the river basins map (Fig. 1) and permission to use it in this article.

This work was performed under financial support of the Russian Foundation for Basic Research, grant 06-05-64464.

References

Baldwin, C.K., Lall, U., 1999. Seasonality of streamflow: the Upper Mississippi River. Water Resour. Res. 35, No. 4, 1143–1154.

Banavar J.R., Colaiori F., Flammini A., Giacometti A., Maritan A., Rinaldo A., 1997. Sculpting of a fractal river basin // Phys. Rev. Lett. 78 (23), 4522–4525.

Banavar J.R., Maritan A., Rinaldo A., 1999. Size and form in efficient transportation networks // Nature 399, 130–132.

Batchelor, G.K., 1970. An Introduction to Fluid Dynamics. Cambridge University Press, Cambridge.

Beran, J., 1994. Statistics for Long-Memory Processes. Chapman and Hall, New York.

Bras, R.L., Rodriguez-Iturbe, I., 1985. Random Functions in Hydrology. Addison-Wesley, Reading, MA.

Cudennec C., Fouad Y., Sumarjo-Gatot I., 2003. Planar organization of river networks: a hidden gamma law structure // Concepts and Modelling in Geomorphology: International Perspectives. Tokyo: TERRAPUB. P. 133–145.

Dahlstedt, K., Jensen, H.J., 2003. Fluctuation spectrum and size scaling of river flow and level. arXiv:cond-mat/0307300 v1.

Dolgonosov, B.M., Gubernatorova, T.N., 2005. A nonlinear model of contaminant transformations in an aquatic environment. Water Resources 32 (3), 291–304.

Dolgonosov, B.M., Gubernatorova, T.N., 2007. Kinetics of the enzymatic decomposition of macromolecules with a fractal structure. Theoretical Foundations of Chemical Engineering 41 (6), 868–877.

Dolgonosov, B.M., Korchagin, K.A., 2005. Probabilistic regularities in unfavorable hydrochemical phenomena. Water Resources 32 (4), 410–416.

Dolgonosov, B.M., Korchagin, K.A., 2007. A nonlinear stochastic model of daily and monthly river flow formation in river basins. Water Resources 34 (6), 624–634.

Dolgonosov, B.M., Korchagin, K.A., Messineva, E.M., 2006. Model of fluctuations in bacteriological indices of water quality. Water Resources 33 (6), 637–650.

Dolgonosov, B.M., Vlasov, D.Yu., Dyatlov, D.V., Suraeva, N.O., Grigorieva, S.V., Korchagin, K.A., 2004. Water quality statistical characteristics at the inlet of water-supply station. Environmental Engineering (Inzhenernaya Ecologia) 3, 2–20.

Feng, X., Kirchner, J.W., Neal, C., 2004. Spectral analysis of chemical time series from long-term catchment monitoring studies: hydrochemical insights and data requirements. Water, Air, and Soil Pollution: Focus 4, 221–235.

Frolov, A.V., 1985. Dynamic Stochastic Models of Perennial Oscillations of Flowthrough Lake Levels. Nauka, Moscow.

Hubert, P., Tchiguirinskaia, I., Bendjoudi, H., Schertzer, D., Lovejoy, S., 2002. Multifractal modeling of the Blavet river discharges at Guerledan // Proceedings of the Third Inter-Celtic Colloquium on Hydrology and Management of Water Resources, National University of Ireland, Galway, 8th-10th July 2002, 131–138.

Hurst, H.E., Black, R.P., Simaika, Y.M., 1965. Long-term Storage: An Experimental Study. Constable, London.

Jensen, H.J., 1998. Self-Organized Criticality. Cambridge University Press, New York, NY.

Klemeš, V., 1973. Watershed as semiinfinitive storage reservoir. J. Irrigation and Drainage. Div. ASCE 99 (4), 477–491.

Klemeš, V., 1974. Probability distribution of outflow a linear reservoir. J. Hydrology 21 (3), 305–414.

Koloshnikova, V.N., Monin, A.S., 1965. Spectra of meteorological field fluctuations. Izvestiya Atmos. Ocean. Phys. 1, 653–669.

Koscielny-Bunde, E., Kantelhardt, J.W., Brown, P., Bunde, A., Havlin, S., 2006. Long-term persistence and multifractality of river runoff records: Detrended fluctuation studies. J. Hydrology 322, 120–137.

Kuchment, L.S., 1980. Models of the River Runoff Formation Processes. Gidrometeoizdat, Leningrad.

Kuzovlev, Yu.E., Bochkov, G.N., 1982. On the origin and statistical parameters of the equilibrium 1/*f*-noise. J. Techn. Phys. Lett. (Pisma v ZhTF) 8 (20), 1260–1263.

Labat, D., Mangin, A., Ababou, R., 2002. Rainfoll-runoff relations for karstic springs: multifractal analyses. J. Hydrology 256, 176–195.

Landau, L.D., Lifshitz, E.M., 1986. Hydrodynamics. Nauka, Moscow.

Lowen, S.B., Teich, M.C., 1993. Fractal renewal processes generate 1/*f*-noise. Phys. Rev. E 47 (2), 992–1001.

Mandelbrot, B.B., Wallis, J.R., 1968. Noah, Joseph, and operational hydrology. Water Resour. Res. 4, 909–918.

Mantilla, R., Gupta, V.K., Mesa, O.J., 2006. Role of couple flow dynamics and real network structures on Yortonian scaling of peak flows. J. Hydrology 322, 155–167.

Maritan A., Rinaldo A., Rigon R., Giacometti A., Rodriguez-Iturbe I., 1996. Scaling laws for river networks // Phys. Rev. E 53 (2), 1510–1515.

Marple, S.L., Jr., 1987. Digital Spectral Analysis with Applications. Prentice-Hall, Englewood Cliffs, N.J.

Naidenov, V.I., 2004. Nonlinear Dynamics of Continental Surface Waters. Nauka, Moscow.

Neal, C., Kirchner, J.W., 2000. Sodium and chloride levels in rainfall, mist, streamwater and groundwater at the Plynlimon catchments, mid-Wales: Inferences on hydrological and chemical controls. Hydrol. Earth Syst. Sci. 4, 295–310.

Pandey, G., Lovejoy, S., Schertzer, D., 1998. Multifractal analysis of daily river flows including extremes for basins of five to two million square kilometers, one day to 75 years. J. Hydrology 208, 62–81.

Pekarova, P., Miklanek, P., Pekar, J., 2003. Spatial and temporal runoff oscillation analysis of the main rivers of the world during the 19th–20th centuries. J. Hydrology 274, 62–79.

Pelletier, J.D., Turcotte, D.L., 1997. Long-range persistence in climatological and hydrological time series: analysis, modeling and application to drought hazard assessment. J. Hydrology 203, 198–208.

Percival, D.B., Walden, A.T., 1993. Spectral Analysis for Physical Applications: Multi-taper and Conventional Univariate Techniques, Cambridge University Press, Great Britain.

Priestley, M.B., 1984. Spectral analysis and time series, Academic Press, London, Third Printing.

Radziejewski, M., Kundzewicz, Z.W., 1997. Fractal analysis of flow of the river Warta. J. Hydrology 200, 280–294.

Rao, A.R., Hamed, K., 2003. Multi-taper method of analysis of periodicities in hydrologic data. J. Hydrology 279, 125–143.

Rinaldo, A., Rodriguez-Iturbe, I., Rigon, R., et al., 1993. Self-organized fractal river networks. Phys. Rev. Lett. 70, 1222–1226.

Rinaldo, A., Banavar, J.R., and Maritan, A., 2006. Trees, networks, and hydrology. Water Resour. Res. 42, W06D07, doi:10.1029/2005WR004108.

Scher, H., Margolin, G., Metzler, R., Klafter, J., Berkowitz, B., 2002. The dynamical foundation of fractal stream chemistry: The origin of extremely long retention times. Geophys. Res. Lett. 29, 10.1029/2001GL014123.

Schepers, H.E., van Beek, J.H.G.M., Bassingthwaighte, J.B., 1992. Four methods to estimate the fractal dimension from self-affine signals. IEEE Engng Med. Bio., June, 57–64.

Shih-I Pai, 1959. Viscous Flow Theory. II–Turbulent Flow. D.Van Nostrand Company, New York.

Schroeder, M.R., 1991. Fractals, Chaos, Power Laws: Minutes from an Infinite Paradise. Freeman, New York.

Spitsyn, I.P., Sokolova, V.A., 1990. General and River Hydraulics. Gidrometeoizdat, Leningrad.

Tessier, Y., Lovejoy, S., Hubert, P., Schertzer, D., Pecknold, S., 1996. Multifractal analysis and modeling of rainfall and river flows and scaling, causal transfer functions. J. Geophys. Res. 31D, 26,427-26,440.

Vladimirov, V.A., Vorobiev, Yu.L., Salov,S.S., et al., 2000. Risk Control: Risk, Sustainable Development, Synergetics. Nauka, Moscow.

Whittle, P., 1962. Topographic correlation, power-law covariance functions, and diffusion. Biometrika 49, 304–314.